Available online at www.sciencedirect.com
SCIENCE DIRECT®
PERGAMON
International Journal of Heat and Mass Transfer 46 (2003) 1563–1573
International Journal of HEAT and MASS TRANSFER
www.elsevier.com/locate/ijhmt

Conjugate heat transfer in inclined open shallow cavities

O. Polat, E. Bilgen *

Ecole Polytechnique, Box 6079, Centre ville, Montreal, Que., Canada H3C 3A7

Received 7 June 2002; received in revised form 5 October 2002

Abstract

Conjugate heat transfer in inclined open shallow cavities has been numerically studied. A thick wall facing the opening is heated by a constant heat flux, sides perpendicular to the heated wall are insulated and the opening is in contact with a fluid at constant temperature and pressure. Conjugate heat transfer by conduction and natural convection is studied by numerically solving equations of mass, momentum and energy. The governing parameters were: Rayleigh numbers, Ra from 10^6 to 10^{12}, conductivity ratio, k_r from 1 to 60, cavity aspect ratio, $A = H/L$ from 1 to 0.125, dimensionless wall thickness, ℓ/L from 0.05 to 0.20 and the inclination angle, φ from 0° to 45° from the horizontal. Isotherms and streamlines are produced, heat and mass transfer is calculated. It is found that volume flow rate, $\dot{V}$ is an increasing function of Ra, A, ℓ/L, φ, and a decreasing function of k_r. Heat transfer, Nu is an increasing function of Ra, ℓ/L, and a decreasing function of k_r. A mixed pattern is found with respect to A and φ. In the former, Nu is an increasing function of the aspect ratio up to a critical Rayleigh number, above which the relationship changes and it becomes a decreasing function of A. In the latter case, Nu is a decreasing function at low Raleigh numbers and an increasing one at high Rayleigh numbers.

Keywords: Conjugate heat transfer; Open shallow cavities; Inclined cavities

1. Introduction

Open cavities are encountered in various engineering systems, such as open cavity solar thermal receivers, uncovered flat plate solar collectors having rows of vertical strips, electronic chips, geothermal reservoirs, etc. For example, in applications such as flat plate solar collectors and electronic chips where small open cavities are formed, the order of magnitude of cavity dimensions is usually small and the temperature difference created by the heat flux is not high. Therefore the heat transfer is usually dominated by laminar natural convection in the cavity. In these applications, often small cavities are formed using fins, which are quasi adiabatic due to symmetry and the wall facing the opening is a plate with finite thickness. The heat flux on the wall is dissipated by natural convection through the open cavity and by conduction through the wall. Hence, a conjugate heat transfer problem exists.

Numerical studies on open cavities have been performed in simulating various applications. Representative studies may be categorized as side facing open cavities with an aspect ratio of one [1–3], similarly inclined open cavities with an aspect ratio of order of one [4], inclined shallow cavities with constant heat flux at the side facing the opening [5] and shallow cavities with small aspect ratio [6]. Similarly experimental studies have been performed using open cavities with an aspect ratio of one [7–9] and shallow cavities [10,11].

Le Quere et al. [1] investigated open isothermal square cavities using primitive variables. Penot [2] investigated the same configuration using stream function-vorticity formulation. Chan and Tien [3], on the other hand, performed a numerical study on an open square cavity with isothermal heated side and adiabatic top and bottom walls. To overcome the difficulties of unknown conditions at the opening, these studies used an

* Corresponding author. Tel.: +1-514-340-4711; fax: +1-514-340-5917.
E-mail address: bilgen@polymtl.ca (E. Bilgen).

0017-9310/03/$ - see front matter
PII: S0017-9310(02)00427-1

Nomenclature

A	enclosure aspect ratio, H/L
c_p	heat capacity, J/kg K
g	acceleration due to gravity, m/s^2
H	cavity height, m
k	thermal conductivity, W/m K
k_r	solid to fluid thermal conductivity ratio, $= k/k_f$
L	cavity width, m
ℓ	wall thickness, m
Nu	Nusselt number, $= hL/k$
p	pressure, Pa
P	dimensionless pressure, $= (p - p_\infty)L^2/\rho\alpha^2$
Pr	Prandtl number, $= v/\alpha$
q''	heat flux, W/m^2
q	dimensionless heat flux, $= -\frac{\partial\theta}{\partial X}$
Ra	Rayleigh number, $= g\beta q'' L^4/(v\alpha k)$
t	time, s
U, V	dimensionless fluid velocities, $= uL/\alpha$, vL/α
$\dot{V}$	dimensionless volume flow rate through the opening
X, Y	dimensionless Cartesian coordinates, $= x/L$, y/L
x, y	Cartesian coordinates

Greek symbols

α	thermal diffusivity, m^2/s
β	volumetric coefficient of thermal expansion, 1/K
v	kinematic viscosity, m^2/s
ρ	fluid density, kg/m^3
ψ	stream function
θ	dimensionless temperature, $= (T - T_\infty)/(Lq''/k)$
φ	inclination angle of the heated wall from the horizontal, °
τ	dimensionless time, $\alpha t/L^2$

Superscripts

$'$	dimensional variables
$\bar{}$	average

Subscripts

a	air
ext	extremum
in	into cavity
max	maximum
min	minimum
out	out of cavity
∞	ambient value
1	section at the solid surface
2	section at the opening

extended domain of computation. Later Chan and Tien [6] investigated open shallow cavity by using the same algorithm but restricting the computation to within the cavity. In comparing with their earlier study with open square cavity [3] and experimental study with open shallow cavity [10], they showed that for an aspect ratio of one, good heat transfer results could be obtained, particularly at high Rayleigh numbers. For shallow cavities, because of greater distance between the end boundaries, the results were even better. Mohamad [4] studied isothermal inclined open cavities with aspect ratio from 0.5 to 2 and showed that the inclination angle did not have any significant effect on the heat transfer rate from the isothermal bottom plate, but substantial one on the local Nusselt number. This aspect was also experimentally investigated by Cha and Choi [9] using an inclined open square cavity, which produced similar findings. Bilgen [11] reported an experimental study with side facing open cavities formed by vertical strips, which had an aspect ratio of about 0.4. The heated side, which was a thick wall, was imposed a constant heat flux while the top and bottom walls were quasi-adiabatic. It was shown that in solar energy applications, the radiation heat exchange could be non-negligible and also natural convection in open cavities heated by a constant heat flux should be addressed excluding and including the radiation effect. Polat and Bilgen [5] studied numerically inclined shallow cavities, with a constant heat flux applied at the side facing the opening and with adiabatic adjoining walls. They showed that heat transfer approached asymptotic values at Rayleigh numbers independent of the aspect ratio. The heat transfer was close to that for a flat plate with constant heat flux. They also found that the effect of elongation of open cavities was to delay this asymptotic behavior.

The literature review shows that conjugate heat transfer problem in these systems has not been addressed. The aim of this study is to examine the conjugate heat transfer in shallow open cavities where the side facing the opening is a thick wall, which is heated by a constant heat flux while the other sides perpendicular to the heated wall are adiabatic.

2. Problem description

A schematic of the two dimensional system with geometrical and boundary conditions is shown in Fig. 1(a). Constant heat flux, q'' is applied on the wall facing the opening and transfered by natural convection to a

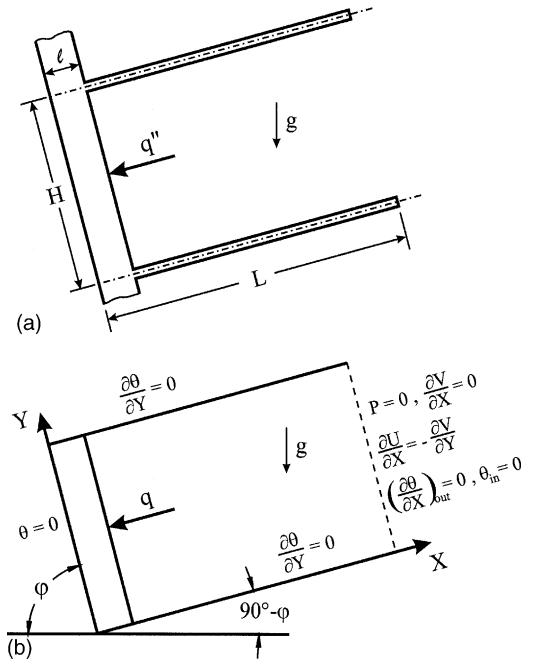

Fig. 1. (a) Schematic of open shallow cavity, (b) coordinate system and boundary conditions.

fluid circulating through the opening to the ambient or a fluid reservoir at a characteristic temperature T'_∞ and through the solid wall by conduction. Other two boundaries of the open cavity are adiabatic.

3. Mathematical model

The continuity, momentum and energy equations for two dimensional laminar flow of an incompressible Newtonian fluid are written. Following assumptions are made: there is no viscous dissipation, the gravity acts in the vertical direction, fluid properties are constant and fluid density variations are neglected except in the buoyancy term (the Boussinesq approximation) and radiation heat exchange is negligible. Using non-dimensional variables defined in the nomenclature, the non-dimensional governing equations are obtained as

$$\frac{\partial U}{\partial X}+\frac{\partial V}{\partial Y}=0 \tag{1}$$

$$\frac{\partial U}{\partial \tau}+U\frac{\partial U}{\partial X}+V\frac{\partial U}{\partial Y}=-\frac{\partial P}{\partial X}+RaPr\theta\cos\varphi + Pr\nabla^2 U \tag{2}$$

$$\frac{\partial V}{\partial \tau}+U\frac{\partial V}{\partial X}+V\frac{\partial V}{\partial Y}=-\frac{\partial P}{\partial Y}+RaPr\theta\sin\varphi+Pr\nabla^2 V \tag{3}$$

$$\frac{\partial \theta}{\partial \tau}+U\frac{\partial \theta}{\partial X}+V\frac{\partial \theta}{\partial Y}=\nabla^2\theta \tag{4}$$

The average and normalized Nusselt numbers are calculated respectively as

$$\left.\begin{aligned}\overline{Nu}&=\frac{-\int_0^A \frac{\partial\theta}{\partial X}\,\mathrm{d}Y}{\int_0^A(\theta_1-\theta_2)}\\ Nu&=\frac{\overline{Nu}_{Ra}}{\overline{Nu}_{Ra=0}}\end{aligned}\right\} \tag{5}$$

The volumetric flow rate is calculated as

$$\left.\begin{aligned}&\dot V=-\int_{X=1}U_{in}\,\mathrm{d}Y\\ &U_{in}=U_{X=1}\ \text{if}\ U_{X=1}<0,\quad U_{in}=0\ \text{if}\ U_{X=1}\geqslant 0\end{aligned}\right\} \tag{6}$$

The stream function is calculated from its definition as

$$U=-\frac{\partial\psi}{\partial Y},\quad V=\frac{\partial\psi}{\partial X} \tag{7}$$

where ψ is zero on the solid surfaces and the streamlines are drawn by $\Delta\psi=(\psi_{\max}-\psi_{\min})/n$ with $n=$ number of increments.

4. Numerical technique

The computational domain was restricted to the cavity with the wall. Hence, the boundary conditions are (see Fig. 1(b))

$$\left.\begin{aligned}&\text{on solid surfaces}\quad U=0,V=0\\ &\text{on adiabatic walls}\quad \tfrac{\partial\theta}{\partial Y}=0\\ &\text{on the wall facing the opening}\quad q=-\tfrac{\partial\theta}{\partial X}\\ &\text{at the opening}\quad P=0,\tfrac{\partial V}{\partial X}=0,\\ &\qquad\qquad \tfrac{\partial U}{\partial X}=-\tfrac{\partial V}{\partial Y},\left(\tfrac{\partial\theta}{\partial X}\right)_{\text{out}}=0,\theta_{\text{in}}=0\end{aligned}\right\} \tag{8}$$

The numerical method used to solve Eqs. (1)–(4) is the semi-implicit method for pressure linked equations revised (SIMPLER) algorithm [13]. The computer code based on the mathematical formulation discussed earlier and the SIMPLER method are validated for various cases published in the literature, the results of which are discussed elsewhere [12].

Uniform grid in X direction of the solid and non-uniform grid elsewhere in X and Y direction were used for all computations. Grid convergence was studied for the case of $A=0.5$ with grid sizes from 30×15 to 120×60 at $Ra=10^{10}$. Grid independence was achieved within 1.17% in Nu and 0.44% in $\dot V$ with a grid size of 60×30. Similar tests were conducted with shallow cavities and the grid size was adjusted accordingly. For example, the grid size for 0.125 aspect ratio was 60×20 for $Ra=10^{10}$. Grid sizes within the computational domain were varied depending on the wall thickness. For example, for $A=0.5$ and $\ell/L=0.10$, it was (10 in

solid + 50 in the cavity) × 30, and for $A = 0.5$ and $\ell/L = 0.20$, (20 in solid + 40 in the cavity) × 30.

Using a P.C. with 1.2 GHz clock speed, the execution time was 48 s for a typical case of $A = 0.5$ and $\ell/L = 0.10$, with a grid size of 60 × 30, $Ra = 10^{10}$ and for 2320 iterations. It was 28 s for $A = 0.125$ and $\ell/L = 0.10$, with a grid size of 60 × 20 and for 2346 iterations.

The accuracy control was carried out by the conservation of mass by setting its variation to less than 10^{-3}, on the pressure term by setting the variation of residues at 10^{-3}. In addition, the accuracy of computations was checked using the energy conservation within the system, by setting its variation to less than 10^{-4}.

4.1. Verification of results with extended computational domain

A study was carried out for verification of the computation technique using a domain restricted to the cavity with a wall, which we may call it the simplified method. The case with $A = 0.50$–0.125, $\ell/L = 0.1$, $k_r = 20$ and for $Ra = 10^8$–10^{11} was studied by taking an extended computational domain, shown in Fig. 2(a). The results are compared with those obtained with the computational domain restricted to the cavity with the wall. Basically, the boundary conditions in the open cavity are the same using both techniques. It is assumed that (i) the extended computational domain is 3L × 9H, (ii) the solid walls in the extended domain making the sides of the open cavity are adiabatic, (iii) the fluid enters from right hand side and exits from the top. We note that the fluid flow simulation in the extended domain could also be accomplished differently, as has been done by others [1–3]. For example, the fluid may be assumed to enter from the bottom and exit from the top. It was seen that the results were similar due to the fact that the far-field boundary conditions did not make too big a difference as long as they were set sufficiently far from the opening. The choice for the present assumption was based on the computational considerations, and to ensure stable and better convergence at high Rayleigh numbers.

Fig. 2(b) shows a comparison of flow and temperature fields for $Ra = 10^{10}$ and Table 1 a comparison of the heat transfer, Nu and the volumetric flow rate through the cavity opening, $\dot{V}$. We see from Fig. 2(b) (i) that the streamlines and isotherms are very similar qualitatively and quantitatively using both computational techniques. $|\Psi_{ext}| = 22.87$ at $X = 1$, $Y = 0.357$ for the restricted domain and 21.39 at $X = 1$, $Y = 0.358$ for the extended domain. The deviations in Nu and $\dot{V}$ in Table 1, particularly at high Rayleigh numbers are acceptable.

We see from Table 1 that the deviations are 18.4% for Nu and 25.9% for $\dot{V}$ at $Ra = 10^8$, they are respectively 4.0% and 17.4% at $Ra = 10^9$, <0.1% and 6.9% at $Ra = 10^{10}$ and 0.7% and 5.7% at $Ra = 10^{11}$. The discrepancy at low Rayleigh numbers, particularly at conduction dominated regime is explained by the fact that in the simplified computational method, the temperature at the opening is set at $\theta = 0$, which in turn increases the temperature gradient. At higher Rayleigh numbers, this effect disappears because a boundary layer type fluid flow and heat transfer establishes, hence the agreement becomes better. At still higher Rayleigh numbers, the

Table 1
Comparison study using restricted and extended computational domains for $A = 0.5$

Ra	Restricted domain		Extended domain	
	Nu	$\dot{V}$	Nu	$\dot{V}$
10^8	1.552	2.085	1.311	1.656
10^9	6.048	8.829	5.816	7.521
10^{10}	14.877	22.869	14.864	21.385
10^{11}	29.691	48.199	29.485	45.588

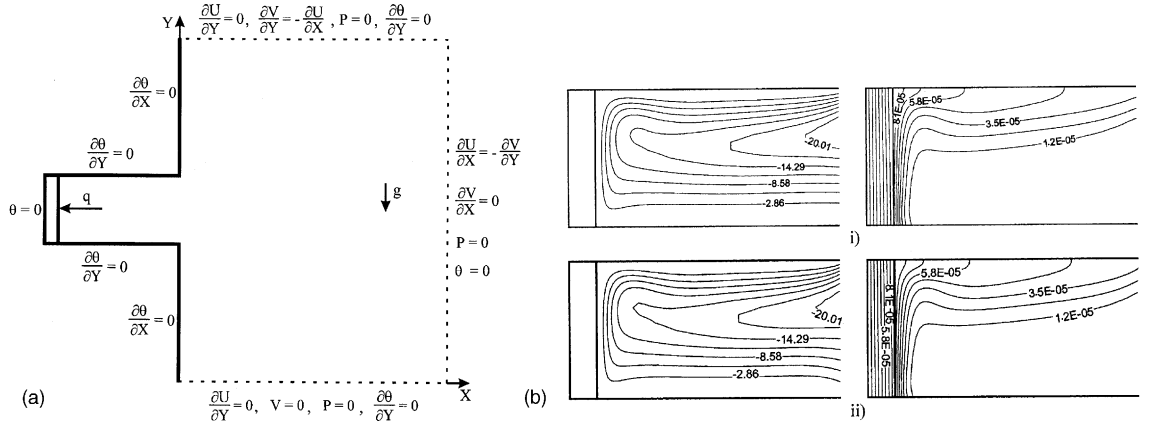

Fig. 2. Comparison study with extended computational domain: (a) schematic of extended domain, (b) streamlines and isotherms for the base case at $Ra = 10^{10}$ using (i) restricted domain, (ii) extended domain.

flow at the corners of the opening is with an angle when extended domain is considered and the simplified method is not able to simulate this situation. These discrepancies are the inherent shortcomings of the simplified method. Despite this, at the range of Rayleigh number considered in this study with a constant heat flux, the approximation is acceptable. A numerical experimentation was also carried out to see the deviations with shallower cases. The results showed that as the cavity became shallower, the deviation became less, since the effect of the far field on the flow and heat transfer in the cavity became less important. For example, for $A = 0.125$ at $Ra = 10^9$ and 10^{10}, the deviations in Nu were 7% and <1% respectively.

We note that the computation time using the extended domain was considerably higher than that with the restricted domain. For example, the same cases discussed earlier are given for comparison: the execution time was 998 s for $A = 0.5$ and $\ell/L = 0.10$, with a grid size of 90×90, $Ra = 10^{10}$ and for 33,000 iterations. It was 73,822 s for $A = 0.125$ and $\ell/L = 0.10$, with a grid size 90×60 and for 1,236,000 iterations. It is seen that considerable economy is achieved by using the computational technique adopted in this study.

5. Results and discussion

Flow and temperature fields, heat transfer and volumetric flow rate through the cavity are examined for ranges of the Rayleigh number from 10^6 to 10^{12}, the aspect ratio from 1 to 0.125 and for φ from 90° (heated wall at vertical position) to 45°. First the results are presented with $\varphi = 90°$ and later the effect of inclination is examined for φ from 90° to 45°. All results are with $Pr = 0.72$. Number of increments is $n = 7$ for both Ψ and θ in the figures.

5.1. General observation

Isotherms and streamlines for $A = 0.5$, $\ell/L = 0.10$ and $k_r = 20$ are presented in Fig. 3(a)–(d) at $Ra = 10^6$ to

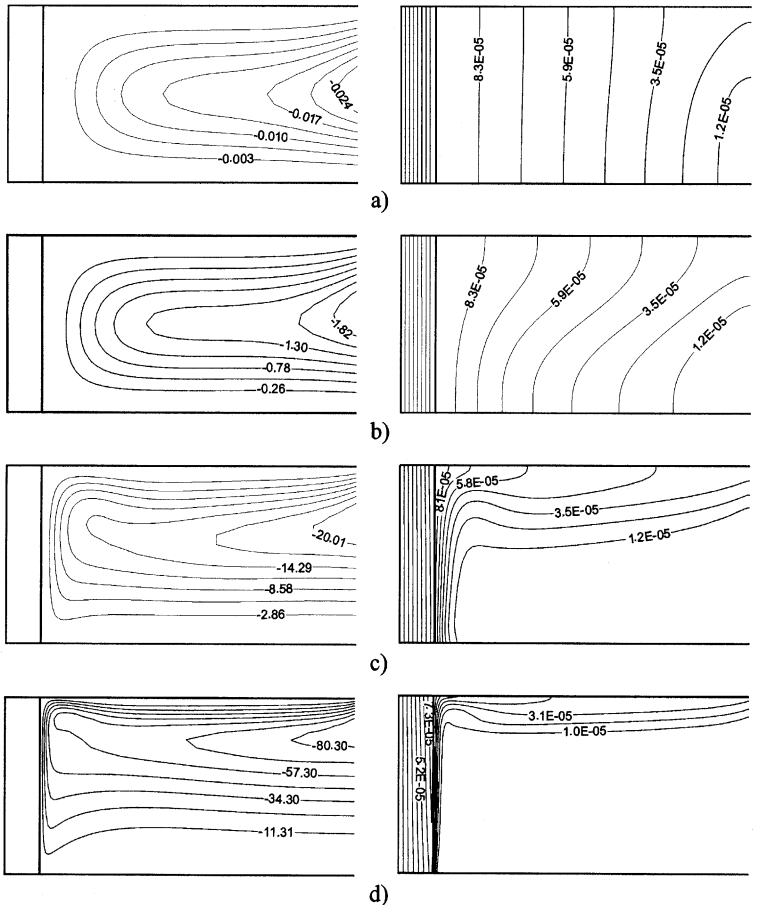

Fig. 3. Streamlines (on the left) and isotherms (on the right) for the base case of $A = 0.5$, $k = 20$, $\ell/L = 0.10$ and $\varphi = 90°$ and various Ra numbers: (a) $Ra = 10^6$, (b) $Ra = 10^8$, (c) $Ra = 10^{10}$ and (d) $Ra = 10^{12}$.

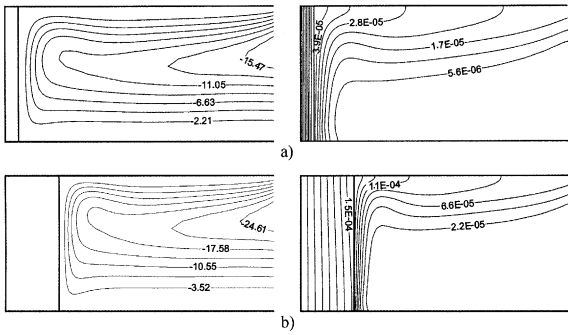

Fig. 4. Streamlines (on the left) and isotherms (on the right) for the case of $A = 0.5$, $k = 20$, $\varphi = 90°$ and $Ra = 10^{10}$, and various ℓ/L: (a) $\ell/L = 0.05$, (b) $\ell/L = 0.20$.

10^{12}, and those for $A = 0.5$ and at $Ra = 10^{10}$ for $\ell/L = 0.05$ and 0.20 in Fig. 4(a)–(b).

We see from Fig. 3(a) that at $Ra = 10^6$ the isotherms show essentially a conduction dominated regime. $|\Psi_{ext}| = 0.028$ at $X = 1$, $Y = 0.278$. At $Ra = 10^8$, Fig. 3(b) shows the case with the isotherms more distorted by the flow, but the temperature gradient is almost constant especially at the lower part of the cavity where the fluid flows following the bottom wall. Compared to the case at $Ra = 10^6$, the convection has increased and it is an equally dominant regime. The isotherms in the solid, as expected, show pure conduction. The streamlines show a parallel flow with a core at the center except at the opening. The flow is clock wise, the fluid is entering from the bottom of the opening and exiting from the top. $|\Psi_{ext}| = 2.08$ at $X = 1$, $Y = 0.278$. As Ra is increased further to 10^{10}, the isotherms in Fig. 3(c) show that the cold fluid penetrates right to the heated wall, where steep temperature gradients exist. The flow becomes similar to boundary layer type. $|\Psi_{ext}| = 22.87$ at $X = 1$, $Y = 0.358$. At $Ra = 10^{12}$, Fig. 3(d) shows that heat transfer and flow is a boundary layer type, the cold fluid penetrates to the heated wall and the convection is rigorous. Flow of the hot fluid exiting from the opening is choked, as a result of which the fluid velocities are increased. $|\Psi_{ext}| = 91.79$ at $X = 1$, $Y = 0.422$. It is also noted that as Ra increases from 10^8 to 10^{12}, the conduction through the solid wall has increasing temperature gradients, showing an increasing heat transfer through it.

Figs. 4(a), 3(c) and 4(b) show the effect of solid wall thickness on the temperature and flow fields for $\ell/L = 0.05$, 0.10 and 0.20 respectively. The flow fields are seen to be similar but the flow becomes more vigorous as the wall thickness increases and it also becomes with steeper gradients near the wall. $|\Psi_{ext}| = 17.68$, 22.87 and 28.13 at $X = 1$ and $Y = 0.333$, 0. 358 and 0.358 for $\ell/L = 0.05$, 0.10 and 0.20 respectively. Similar observations apply for the temperature fields. It is seen that the temperature gradients are higher near the wall for increasing ℓ/L. These observations are expected, for as the wall thickness increases, the wall conductance decreases and the heat transfer through the solid wall decreases. As a result, the heat transfer by convection becomes increased.

5.2. Temperature and velocity profiles

Non-dimensional temperature profiles on the heated wall ($\ell/L = 0.10$) and at the opening, and the velocity profile at the opening at $Ra = 10^{10}$ are shown in Fig. 5(a) and (b) for $A = 0.5$ and 0.125 respectively. It is seen in both cases that the heated wall temperature follows a non-linear variation, a little lower near the bottom and

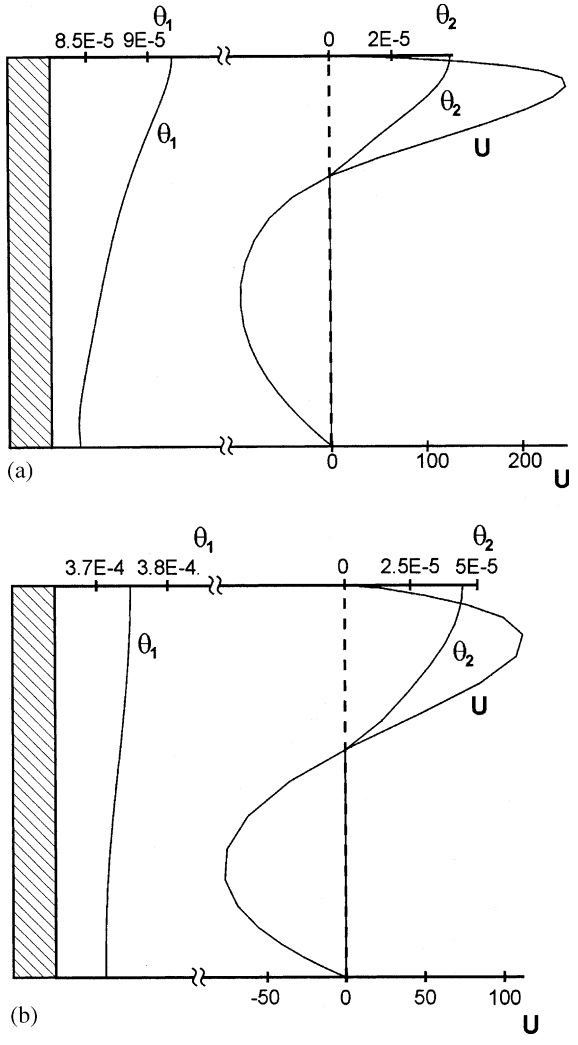

Fig. 5. Non-dimensional temperature profiles on the heated wall and at the opening, and the horizontal velocity profile at the opening for the case with $k = 20$, $\ell/L = 0.10$ and $\varphi = 90°$ at $Ra = 10^{10}$: (a) $A = 0.5$ and (b) $A = 0.125$.

higher at the top. The cold fluid entering the cavity is heated along the wall, cooling it more effectively at lower elevations. As the heated fluid convects along the wall, the wall temperature also increases. As expected, due to thermal mass of the wall, its temperature is not affected too much. The temperature profile at the opening shows that the temperature is $\theta = 0$ at the lower portion where the fluid enters the cavity and hot fluid exits at the remaining upper portion.

The outgoing flow occupies 30% of the opening with $A = 0.5$ while 41% with $A = 0.125$. This is related to the volume flow rate for each case and is consistent with the observation made with streamlines in Figs. 3 and 4.

5.3. Volume flow rate and heat transfer

Normalized heat transfer, *Nu* and non-dimensional volume flow rate in and out the cavity, $\dot{V}$ have been calculated using Eqs. (5) and (6) for various cases and as a function of *Ra* number, ℓ/L, k_r and A. A base case with $A = 0.5$, $k = 20$ and $\ell/L = 0.10$ has been considered and each parameter is in turn treated as a variable parameter. They are presented in Figs. 6–11, which will be discussed next.

Nu and $\dot{V}$ as a function of *Ra* are shown in Fig. 6 with A as a parameter. Generally, $\dot{V}$ is an increasing function of *Ra* and A. As expected, at a given *Ra*, shallower the cavity, smaller is the volumetric flow rate. It is seen that for a given A, the relative increase in $\dot{V}$ is smaller at low *Ra* numbers than at high *Ra* numbers. It is seen that the volumetric flow rates for different aspect ratios appear to become asymptote to a line for which the aspect ratio $A \to \infty$, i.e. a vertical flat wall. In fact, a test with $A = 10$ showed that this might be the case.

Normalized Nusselt number is calculated using Eq. (5), which is equal to unity for purely conduction heat transfer. For shallower cavities, conduction regime may dominate the heat transfer even at high *Ra* numbers, such is the case for $A = 0.125$ with a transition from conduction to convection regime at $Ra = 10^9$. The transition *Ra* number for each aspect ratio is lower for increasing A. Up to $Ra = 10^9$, *Nu* is an increasing function of A at which value a mixed pattern emerges and continues until $Ra \approx 2 \times 10^{11}$. For example at $Ra \approx 10^9$, for $A = 0.5$, *Nu* becomes higher than that for $A = 1$ and similarly for other cases with smaller A. At $Ra \approx 2 \times 10^{11}$, it appears that the heat transfer, *Nu* becomes a decreasing function of A. The reason is as follows: At a given *Ra*, the heat flux is constant. A part of heat, q_1 is transferred by conduction through the wall and the other, q_2 by convection through the opening. At low Rayleigh numbers, for shallow cavities, heat transfer is dominated by conduction regime. Therefore, shallower the cavity, smaller is the part convected. i.e., the relative heat transfer by convection, $q_2/(q_1 + q_2)$ is smaller,

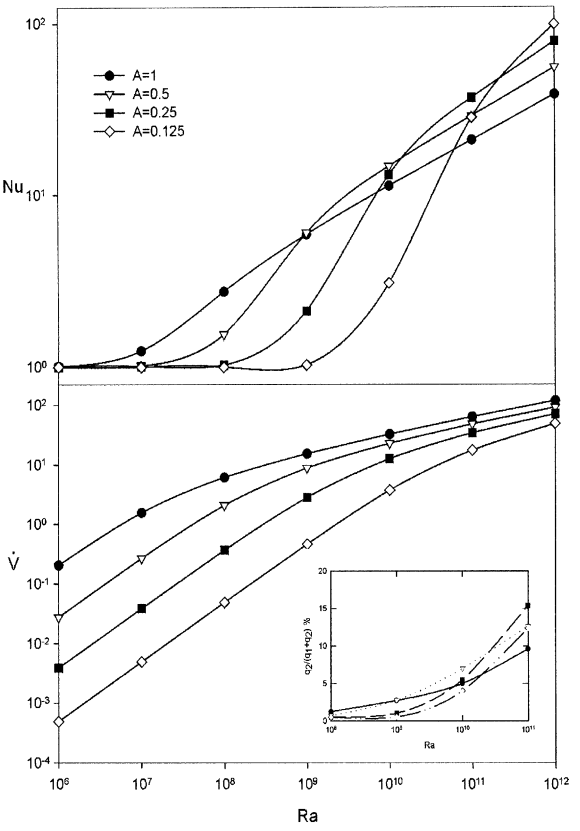

Fig. 6. Normalized Nusselt number and volume flow rate as a function of Rayleigh number with the aspect ratio as a parameter for the case with $\ell/L = 0.10$, $k_r = 20$, $\varphi = 90°$.

hence *Nu* is relatively smaller. At high Rayleigh numbers, the convection becomes rigorous, as a result of which the heat transfer by convection, $q_2/(q_1 + q_2)$ becomes relatively important for shallow cavities. As Rayleigh number increases, the relative increase in convection becomes higher as the cavity becomes shallower. For example, at *Ra* between 10^9 and 10^{10}, the relative increase in convection is 2.12 times for $A = 1$ and 4.48 times for $A = 0.25$. We see that *Nu* for the latter exceeds that of the former at $Ra = 10^{10}$. The relative increase $q_2/(q_1 + q_2)$ as a function of *Ra* is shown in the insert of Fig. 6.

The relative increase in convection is directly related to the variation of Nusselt number observed in Fig. 6. For example, at $Ra = 10^8$, for $A = 1$, 0.5, 0.25 and 0.125, the relative heat transfer by convection, $q_2/(q_1 + q_2)$ is 1.24%, 0.73%, 0.51% and 0.51% respectively. Following these relative values, we see that *Nu* for $A = 1$ is the highest, then it is for $A = 0.5$, and *Nu* is almost the same for $A = 0.25$ and 0.125. At $Ra = 10^9$, $q_2/(q_1 + q_2)$ is 2.74%, 2.77%, 1.04% and 0.53% respectively. Following these relative values, *Nu* is almost the same for $A = 1$ and

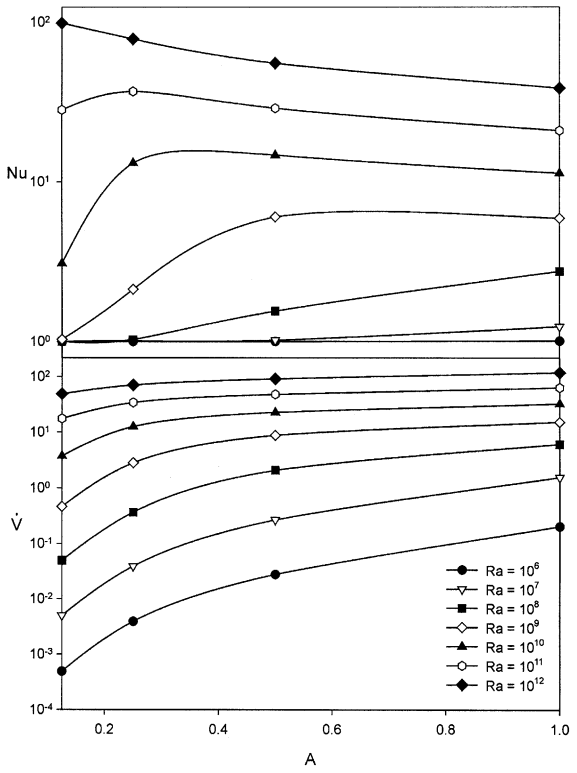

Fig. 7. Normalized Nusselt number and volume flow rate as a function of the aspect ratio with Rayleigh as a parameter for the case with $\ell/L = 0.10$, $k_r = 20$, $\varphi = 90°$.

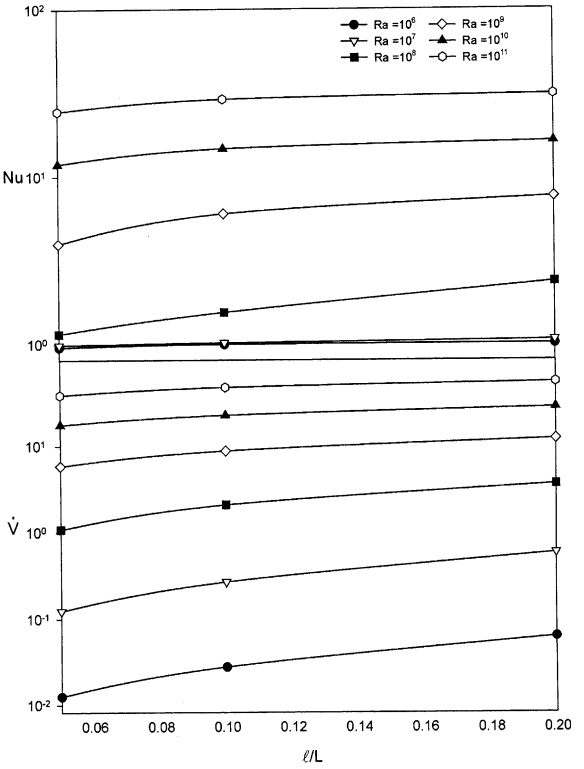

Fig. 8. Normalized Nusselt number and volume flow rate as a function of the dimensionless wall thickness, ℓ/L with Rayleigh as a parameter for the case with $A = 0.5$, $k_r = 20$, $\varphi = 90°$.

0.5 in Fig. 6. At still higher Rayleigh numbers, at $Ra = 10^{11}$ for example, $q_2/(q_1 + q_2)$ is 9.60%, 12.65%, 15.35% and 12.36% respectively. The relative heat transfer by convection shows that the lowest *Nu* is for $A = 1$, then, it is for $A = 0.5$ and 0.125, which is almost equal and the highest is for $A = 0.25$.

The observed phenomenon regarding heat transfer by convection in Fig. 6 is new and has not been observed earlier in shallow cavities without a massive wall. In fact, earlier studies with isothermal [3] and constant heat flux [5] at the boundary facing the opening showed that following the trend with the volume flow rate, the heat transfer by convection was asymptote to the case of a vertical flat plate.

As a result of the mixed pattern observed for *Nu*, if we examine *Nu* as a function of *A*, for $Ra = 10^6$–10^{12} as a parameter, we can see in Fig. 7 that for a given *Ra*, *Nu* is maximized at an optimum aspect ratio *A*. The optimum *A* shifts to lower values for increasing *Ra*, as we can see clearly for the cases of $Ra = 10^9$–10^{11}. The optimum aspect ratio is about 0.25 at $Ra = 10^{11}$, 0.35 at $Ra = 10^{10}$ and 0.6 at $Ra = 10^9$. We also see that the volume flow rate, $\dot{V}$ is an increasing function of *A* for any Rayleigh number. Although it is a strong function at low *Ra*, it becomes less sensitive as *Ra* is increased, a trend which is also observed in Fig. 6.

The effect of wall thickness, ℓ/L on $\dot{V}$ and *Nu* is shown in Fig. 8 for various *Ra* numbers. Similar to our observation with Fig. 7, the volumetric flow rate is an increasing function of the wall thickness at all Rayleigh numbers. Its effect is large in conduction dominated regime and becomes small at high *Ra* numbers. Similar observations apply also for Nusselt number. The observed results are due to the fact that the conductance decreases with increasing wall thickness, as a result, the applied heat flux becomes dissipated more by convection in the open cavity and a smaller part goes through the wall. This phenomenon is enhanced at low Rayleigh numbers for the reason that convection in the high conductance case is weak and any decrease in conductance causes an increased convection in the open cavity.

The effect of conductivity ratio, k_r on $\dot{V}$ and *Nu* is presented in Fig. 9 with *Ra* as a parameter. It is seen that both volumetric flow rate and Nusselt number are negatively and similarly affected for increasing conductivity ratio. For $k_r = 1$, i.e., for an insulating material both $\dot{V}$ and *Nu* are higher, since the heat flux applied at the wall is mostly convected through the open cavity. As the

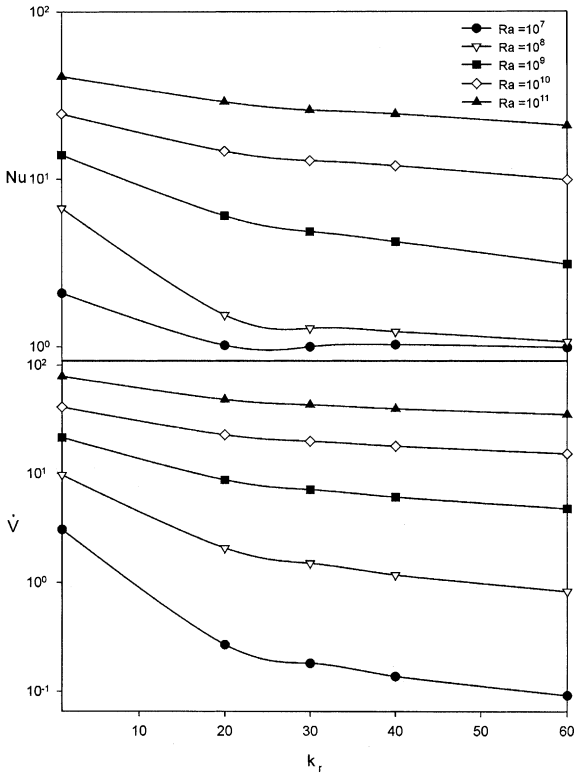

Fig. 9. Normalized Nusselt number and volume flow rate as a function of the conductivity ratio, k_r with Rayleigh as a parameter for the case with $A = 0.5$, $\ell/L = 0.10$, $\varphi = 90°$.

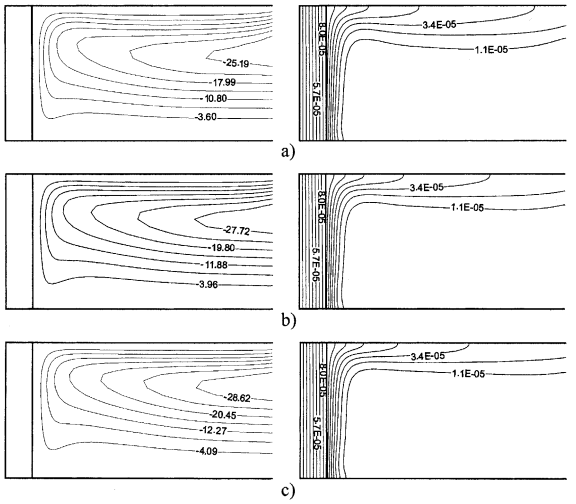

Fig. 10. Streamlines (on the left) and isotherms (on the right) for the case with $A = 0.5$, $k = 20$, $\ell/L = 0.10$ at $Ra = 10^{10}$, and various φ: (a) $\varphi = 75°$, (b) $\varphi = 60°$ and (c) $\varphi = 45°$.

conductivity of the wall increases, a part of the applied heat flux goes through the wall and as a result, the

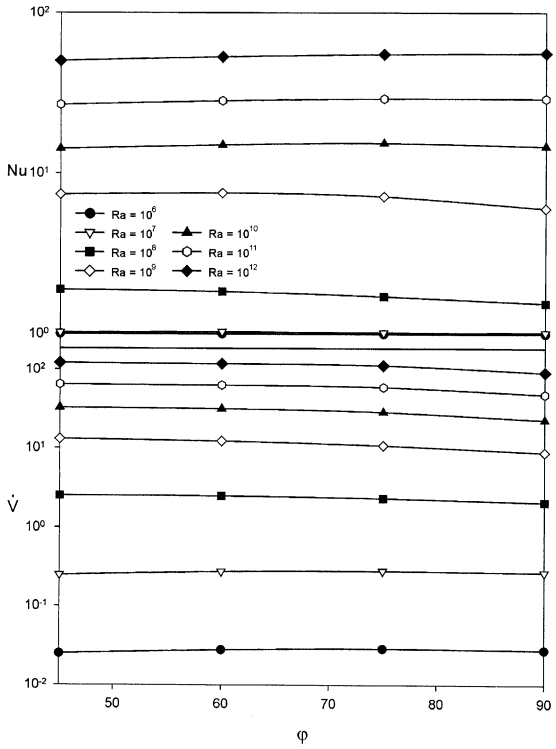

Fig. 11. Normalized Nusselt number and volume flow rate as a function of the inclination angle φ and Rayleigh as a parameter for the case with $A = 0.5$, $\ell/L = 0.10$, $k_r = 20$.

convected heat transfer becomes less. Also for the same reason, the volumetric flow rate becomes less.

The results of Figs. 6–9 show that with the parameters of the base case, the heat transfer by convection is a small part of the total even at high Rayleigh numbers and the major part is transfered by conduction through the wall to the left. Therefore, in applications where the aim is to transfer heat to the left and suppress convection to the right, shallow cavities with wall having high conductance should be used.

5.4. Effect of inclination angle

The effect of inclination angle is examined for φ from 90° to 45° and with $A = 0.5$ and 0.25, covering practical cases in solar collectors and other applications. Isotherms and streamlines for a typical case with $A = 0.5$ and $Ra = 10^{10}$ are presented in Fig. 10 for 75°, 60° and 45° inclination of the heated wall from the horizontal. The case with $\varphi = 90°$ is presented in Fig. 3(c). Isotherms and streamlines show that as the inclination angle of the heated plate decreases, the velocity gradient increases at upper adiabatic wall, the strength of the circulation increases. In fact, streamlines on the left show that $|\Psi_{ext}| = 28.79$, 31.68 and 32.71 at $X = 1$,

$Y = 0.333$ at $\varphi = 75°$, 60°, 45° respectively. Compared to the base case with $\varphi = 90°$, $|\Psi_{ext}|$ increases considerably making the convection more rigorous when the heated wall is inclined further. Flow of the hot fluid from the opening is choked as the inclination is decreased, as a result of which the fluid velocities are increased. Isotherms show that the temperature gradient is also similarly affected. The temperature gradients are clearly increased as the opening is positioned upwards. Therefore, as expected, the volumetric flow rate and heat transfer should increase with decreasing inclination angle of the heated plate. Similar observations were made with $A = 0.25$ for the same inclination angles with strength of convection relatively more vigorous than with $A = 0.5$.

For $A = 0.5$, volumetric flow rate and heat transfer as a function of inclination angle are shown in Fig. 11 with Ra as a parameter. It is seen that the volumetric flow rate increases with decreasing inclination angle of the heated wall or when the opening faces upward from the horizontal. It is noted that $(90° - \varphi)$ is the slope of the open cavity as shown in Fig. 1(b). At low Rayleigh numbers, the increase is small however as the Rayleigh number increases, the increase of volume flow rate also becomes considerable. The relative change varies from about -7.5% to 48.94%, both corresponding to $\varphi = 45°$ at $Ra = 10^7$ and $Ra = 10^9$ respectively. For $A = 0.25$, it was seen that a similar observation could be made. The variation of the relative change in $\dot{V}$ was however more discernible, from -0.5% to 40.42%, corresponding to $\varphi = 45°$ at $Ra = 10^8$ and 10^9 respectively.

Heat transfer for the case $A = 0.5$ is shown at the upper part of Fig. 11. It is seen that similar to the observation made with the volumetric flow rate at low Rayleigh numbers, the heat transfer is conduction dominated upto 10^8. For $Ra > 10^8$, Nu increases with decreasing φ at $Ra = 10^8$ with a maximum at $\varphi = 45°$ at which the relative change is 19.63%. At $Ra = 10^9$, it increases with a maximum at $\varphi = 60°$ at which the relative change is 25.05%. At $Ra = 10^{10}$ and 10^{11}, the maximum is at $\varphi = 75°$ with relative change of 4.96% and 0.84% respectively. Similar observations were made with $A = 0.25$, but the variation of the relative increase was up to 8.17% for $Ra = 10^{11}$ and $\varphi = 75°$.

6. Conclusions

Laminar natural convection in inclined open shallow cavities has been numerically studied for the case of constant heat flux at the end wall and adiabatic at the boundaries perpendicular to the heated wall. Equations of mass, momentum and energy have been solved using constant properties and Boussinesq approximation. The computation domain has been restricted to the cavity and approximate boundary conditions at the opening have been assumed. Isotherms, streamlines, and temperature and velocity profiles have been produced. The volume flow rate in and out the cavity and heat transfer as a function of Rayleigh number, and various other parameters have been obtained. It is found that (i) using a computational domain restricted to the cavity, assuming appropriate boundary conditions, could produce results within few percent deviation from those obtained with an extended computational domain, (ii) the volume flow rate is an increasing function of Rayleigh number and the aspect ratio, (iii) the heat transfer is an increasing function of the aspect ratio and Rayleigh number for low Rayleigh numbers. For a given aspect ratio, a mixed pattern emerges in which this trend changes: the heat transfer becomes a decreasing function of it at a critical Ra number, which is at a higher value as the aspect ratio becomes smaller. As a result of this mixed pattern, Nusselt number is maximized at an optimum aspect ratio at a given Rayleigh number, (iv) the volume flow rate and the heat transfer are an increasing function of both the dimensionless wall thickness and Rayleigh number, (v) the volume flow rate and the heat transfer are a decreasing function of the dimensionless conductivity ratio and an increasing function of Rayleigh number, (vi) at high Rayleigh numbers, the volume flow rate is a decreasing function of the inclination angle of the wall while the heat transfer is an increasing function of it. At low Rayleigh numbers, the functional relationship reverses.

Acknowledgements

We would like to express our sincere thanks to Dr. R. Ben Yedder for his valuable assistance in the numerical experimentation with restricted and extended domains, and in using the calculation code. Financial support by Natural Sciences and Engineering Research Council of Canada is acknowledged.

References

[1] P. Le Quere, J.A.C. Humphrey, F.S. Sherman, Numerical calculation of thermally driven two-dimensional unsteady laminar flow in cavities of rectangular cross section, Numer. Heat Transfer 4 (1981) 249–283.
[2] F. Penot, Numerical calculation of two-dimensional natural convection in isothermal open cavities, Numer. Heat Transfer 5 (1982) 421–437.
[3] Y.L. Chan, C.L. Tien, A numerical study of two-dimensional natural convection in square open cavities, Numer. Heat Transfer 8 (1985) 65–80.
[4] A.A. Mohamad, Natural convection in open cavities and slots, Numer. Heat Transfer 27 (1995) 705–716.
[5] O. Polat, E. Bilgen, Laminar natural convection in inclined open shallow cavities, Int. J. Therm. Sci. 41 (2002) 360–368.

[6] Y.L. Chan, C.L. Tien, A numerical study of two-dimensional laminar natural convection in shallow open cavities, Int. J. Heat Mass Transfer 28 (3) (1985) 603–612.
[7] V. Sernas, I. Kyriakides, Natural convection in an open cavity, in: Proc. Seventh Int. Heat Transfer Conf., Munich, vol. 2, 1982, pp. 275–286.
[8] C.F. Hess, R.H. Henze, Experimental investigation of natural convection losses from open cavities, J. Heat Transfer 106 (1984) 333–338.
[9] S.S. Cha, K.J. Choi, An interferometric investigation of open cavity natural convection heat transfer, Exp. Heat Transfer 2 (1989) 27–40.
[10] Y.L. Chan, C.L. Tien, Laminar natural convection in shallow open cavities, J. Heat Transfer 108 (1986) 305–309.
[11] E. Bilgen, Passive solar massive wall systems with fins attached on the heated wall and without glazing, J. Solar Energy Eng. 122 (2000) 30–34.
[12] R. Ben Yedder, E. Bilgen, Laminar natural convection in inclined enclosures bounded by a solid wall, Heat Mass Transfer 32 (1997) 455–462.
[13] S.V. Patankar, Numerical Heat Transfer and Fluid Flow, Hemisphere Publishing Corporation, New York, 1980.